Article

Resistive-Pulse Studies of Proteins and Protein/Antibody Complexes Using a Conical Nanotube Sensor

Lindsay T. Sexton, Lloyd P. Horne, Stefanie A. Sherrill, Gregory W. Bishop, Lane A. Baker, and Charles R. Martin

J. Am. Chem. Soc., **2007**, 129 (43), 13144-13152• DOI: 10.1021/ja0739943 • Publication Date (Web): 06 October 2007

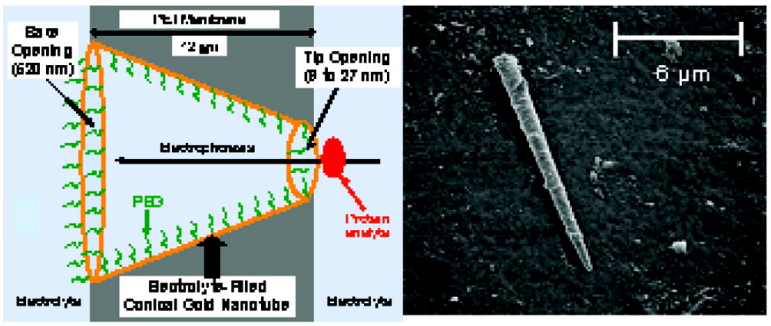

More About This Article

Additional resources and features associated with this article are available within the HTML version:

- Supporting Information
- Links to the 6 articles that cite this article, as of the time of this article download
- Access to high resolution figures
- Links to articles and content related to this article
- Copyright permission to reproduce figures and/or text from this article

View the Full Text HTML

J|A|C|S
ARTICLES
Published on Web 10/06/2007

Resistive-Pulse Studies of Proteins and Protein/Antibody Complexes Using a Conical Nanotube Sensor

Lindsay T. Sexton, Lloyd P. Horne, Stefanie A. Sherrill, Gregory W. Bishop, Lane A. Baker,† and Charles R. Martin*

Contribution from the Department of Chemistry and Center for Research at the Bio/Nano Interface, University of Florida, Gainesville, Florida 32611-7200

Received June 1, 2007; E-mail: crmartin@chem.ufl.edu

Abstract: There is increasing interest in using nanopores in synthetic membranes as resistive-pulse sensors for molecular and macromolecule analytes. In general, this method entails measuring current pulses associated with translocation of the analyte through the nanopore sensor element. A key challenge for this sensing paradigm is building selectivity into the protocol so that the current pulses for the target analyte can be distinguished from current pulses for other species that might be present in the sample. We show here that this can be accomplished with a protein analyte by adding to the solution an antibody that selectively binds the protein. We demonstrate this concept using bovine serum albumin (BSA) and a Fab fragment from a BSA-binding polyclonal antibody. Because the complex formed upon binding of the Fab to BSA is larger than the free BSA molecule, the current-pulse signature for the BSA/Fab complex can be easily distinguished from the free BSA. Furthermore, the BSA/Fab pulses can be easily distinguished from the pulses obtained for the free Fab and from pulses obtained for a control protein that does not bind to the Fab. Finally, we also show that the current-pulse signature for the BSA/Fab complex can provide information about the size and stoichiometry of the complex.

Introduction

There is increasing interest in using nanopores in synthetic[1−21] or biological[22−39] membranes as resistive-pulse sensors for molecular and macromolecule analytes.[1−39] The resistive-pulse method,[1] which when applied to such analytes is sometimes called stochastic sensing,[22−30] entails mounting the membrane containing the nanopore between two electrolyte solutions, applying a transmembrane potential difference, and measuring the resulting ion current flowing through the electrolyte-filled

† Current address: Department of Chemistry, Indiana University, Bloomington, IN 47405-7102.

(1) Martin, C. R.; Bayley, H. *Chem. Rev.* **2000**, *100*, 2575−2594.
(2) Henriquez, R. R.; Ito, T.; Sun, L.; Crooks, R. M. *The Analyst* **2004**, *129*, 478−482.
(3) Choi, Y.; Baker, L. A.; Hillebrenner, H.; Martin, C. R. *Phys. Chem. Chem. Phys.* **2006**, *8*, 4976−4988.
(4) Siwy, Z. S.; Trofin, L.; Kohli, P.; Baker, L. A.; Trautmann, C.; Martin, C. R. *J. Am. Chem. Soc.* **2005**, *127*, 5000−5001.
(5) Park, S. R.; Peng, H.; Ling, X. S. *Small* **2007**, *3*, 116−119.
(6) Harrell, C. C.; Choi, Y.; Horne, L. P.; Baker, L. A.; Siwy, Z. S.; Martin, C. R. *Langmuir* **2006**, *22*, 10837−10843.
(7) Heins, E. A.; Siwy, Z. S.; Baker, L. A.; Martin, C. R. *Nano Lett.* **2005**, *5*, 1824−1829.
(8) Saleh, O. A.; Sohn, L. L. *Nano Lett.* **2003**, *3*, 37−38.
(9) Saleh, O. A.; Sohn, L. L. *Proc. Natl. Acad. Sci. U.S.A.* **2003**, *100*, 820−824.
(10) Li, J.; Stein, D.; McMullan, C.; Branton, D.; Aziz, M. J.; Golovchenko, J. A. *Nature* **2001**, *412*, 166−169.
(11) Li, J.; Gershow, M.; Stein, D.; Brandin, E.; Golovchenko, J. A. *Nat. Mater.* **2003**, *2*, 611−615.
(12) Fologea, D.; Gershow, M.; Ledden, B.; McNabb, D. S.; Golovchenko, J. A.; Li, J. *Nano Lett.* **2005**, *5*, 1905−1909.
(13) Chen, P.; Mitsui, T.; Farmer, D. B.; Golovchenko, J.; Gordon, R. G.; Branton, D. *Nano Lett.* **2004**, *4*, 1333−1337.
(14) Chen, P.; Gu, J.; Brandin, E.; Kim, Y. R.; Wang, Q.; Branton, D. *Nano Lett.* **2004**, *4*, 2293−2298.
(15) Han, A.; Schurmann, G.; Mondin, G.; Bitterli, R. A.; Hegelbach, N. G.; de Rooij, N. F.; Staufer, U. *Appl. Phys. Lett.* **2006**, *88*, 093901−1.
(16) Storm, A. J.; Chen, J. H.; Ling, X. S.; Zandbergen, H. W.; Dekker, C. *Nat. Mater.* **2003**, *2*, 537−540.
(17) Storm, A. J.; Chen, J. H.; Zandbergen, H. W.; Dekker, C. *Phys. Rev. E* **2005**, *71*, 051903.
(18) Sun, L.; Crooks, R. M. *J. Am. Chem. Soc.* **2000**, *122*, 12340−12345.
(19) Uram, J. D.; Ke, K.; Hunt, A. J.; Mayer, M. *Angew. Chem., Int. Ed.* **2006**, *45*, 2281−2285.
(20) Chang, H.; Kosari, F.; Andreadakis, G.; Alam, M. A.; Vasmatzis, G.; Bashir, R. *Nano Lett.* **2004**, *4*, 1551−1556.
(21) Smeets, R. M.; Keyser, U. F.; Krapf, D.; Wu, M. Y.; Dekker, N. H.; Dekker, C. *Nano Lett.* **2006**, *6*, 89−95.
(22) Bayley, H.; Cremer, P. S. *Nature* **2001**, *413*, 226−230.
(23) Gu, L. Q.; Braha, O.; Conlan, S.; Cheley, S.; Bayley, H. *Nature* **1999**, *398*, 686−690.
(24) Howorka, S.; Cheley, S.; Bayley, H. *Nat. Biotechnol.* **2001**, *19*, 636−639.
(25) Kasianowicz, J. J.; Burden, D. L.; Han, L. C.; Cheley, S.; Bayley, H. *Biophys. J.* **1999**, *76*, 837−845.
(26) Braha, O.; Gu, L. Q.; Zhou, L.; Lu, X.; Cheley, S.; Bayley, H. *Nat. Biotechnol.* **2000**, *18*, 1005−1007.
(27) Astier, Y.; Braha, O.; Bayley, H. *J. Am. Chem. Soc.* **2006**, *128*, 1705−1710.
(28) Guan, X.; Gu, L. Q.; Cheley, S.; Braha, O.; Bayley, H. *Chem. Biol. Chem.* **2005**, *6*, 1875−1881.
(29) Howorka, S.; Nam, J.; Bayley, H.; Kahne, D. *Angew. Chem., Int. Ed.* **2004**, *43*, 842−846.
(30) Movileanu, L.; Howorka, S.; Braha, O.; Bayley, H. *Nat. Biotechnol.* **2000**, *18*, 1091−1095.
(31) Bezrukov, S. M.; Vodyanoy, I.; Brutyan, R. A.; Kasianowicz, J. J. *Macromolecules* **1996**, *29*, 8517−8522.
(32) Henrickson, S. E.; Misakian, M.; Robertson, B.; Kasianowicz, J. J. *Phys. Rev. Lett.* **2000**, *85*, 3057−3060.
(33) Kasianowicz, J. J.; Henrickson, S. E.; Weetall, H. H.; Robertson, B. *Anal. Chem.* **2001**, *73*, 2268−2272.
(34) Kasianowicz, J. J.; Brandin, E.; Branton, D.; Deamer, D. W. *Proc. Natl. Acad. Sci. U.S.A.* **1996**, *93*, 13770−13773.
(35) Meller, A.; Nivon, L.; Brandin, E.; Golovchenko, J. ; Branton, D. *Proc. Natl. Acad. Sci. U.S.A.* **2000**, *97*, 1079−1084.
(36) Meller, A.; Nivon, L.; Branton, D. *Phys. Rev. Lett.* **2001**, *86*, 3435−3438.
(37) Meller, A.; Branton, D. *Electrophoresis* **2002**, *23*, 2583−2591.
(38) Deamer, D. W.; Branton, D. *Acc. Chem. Res.* **2002**, *35*, 817−825.
(39) Bezrukov, S. M.; Kullman, L.; Winterhalter, M. *FEBS Lett.* **2000**, *476*, 224−228.

10.1021/ja0739943 CCC: $37.00

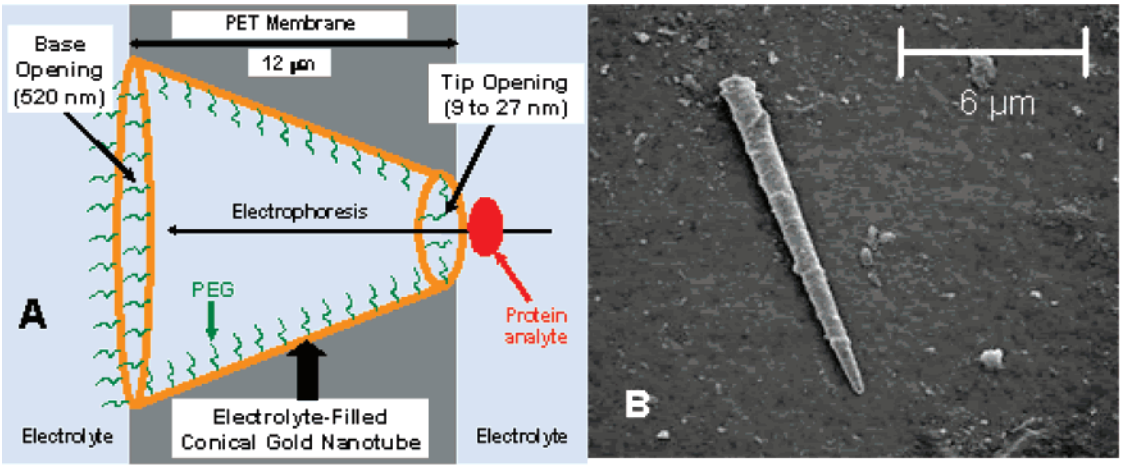

Figure 1. (A) Schematic of the PEG-functionalized conical gold nanotube sensor element, showing the base-opening and tip-opening diameters used in these studies. Not to scale. (B) Electron micrograph of such a sensor element after removal from the PET membrane. Note that in the sensing experiment, the nanotube is left embedded in the PET membrane, but it was removed here so that it could be imaged.

nanopore. In simplest terms, when the analyte enters and translocates the nanopore, it transiently blocks the ion current, resulting in a downward current pulse. The current-pulse frequency is proportional to the concentration of the analyte, and the identity of the analyte is encoded in the current-pulse signature, as defined by the average magnitude and duration of the current pulses.[1−39]

A key challenge is building analyte selectivity into the sensor itself or into the sensing protocol. For sensors based on the biological nanopore α-hemolysin, this has been accomplished by attaching an analyte-selective molecular-recognition agent (MRA) to the nanopore.[22−30] When the analyte is present, it binds to this MRA, yielding current pulses of duration determined by the chemical kinetics of the analyte/MRA interaction. As a result, the current-pulse duration for the analyte is, in general, longer than those for species that do not bind to the MRA. While we have attached MRAs to artificial nanotubes to make highly selective protein sensors, these devices did not use the resistive-pulse method.[4]

Another approach for introducing analyte selectivity entails attaching the MRA to a pore-translocating "reporter" species instead of to the nanopore itself.[9,33] The reporter is first sent through the nanopore in the absence of the analyte to yield current pulses characteristic of the free reporter. When the analyte is subsequently added, it binds to the MRA on the reporter. Because the resulting reporter/analyte complex is larger in size, the current-pulse signature changes in a predictable way (e.g., longer duration pulses are observed), and it is this change that signals selective detection of the analyte by the MRA-functionalized reporter.[9,33]

We investigate here a related strategy for introducing analyte selectivity to resistive-pulse sensing.[19] While this method also makes use of an analyte-selective MRA, it does not require attachment of the MRA to a reporter species. Instead, the MRA used is of dimensions comparable to those of the analyte to be detected. The analyte is first sent through the sensor to obtain current pulses for the free analyte. The MRA is then added to yield the analyte/MRA complex, which is then sent through the sensor. Because the complex is larger than either the free analyte or the free MRA, longer duration current pulses are observed, which signals selective detection of the analyte. We prove this concept here using bovine serum albumin (BSA) as the analyte and a Fab fragment from an antibody to BSA (anti-BSA-Fab) as the MRA. The sensor element was a poly(ethylene glycol) (PEG)-functionalized[40,41] conical gold nanotube[4] prepared by the track-etch method[42,43] in a poly(ethylene terephthalate) (PET) membrane (Figure 1).

Experimental Section

Materials. The anti-BSA-Fab was obtained from Sigma Aldrich; SDS-PAGE showed it to have a molecular weight (MW) of ∼50 kDa. BSA (MW ∼66 kDa) was obtained from Sigma Aldrich, as was the control protein streptavidin (SA, MW ∼60 kDa). Poly(ethylene terephthalate) (PET) membranes, 12 μm thick, which contained a single heavy-ion induced damage track, were obtained from GSI (Darmstadt, Germany). A thiolated poly(ethylene glycol) (PEG-thiol, MW 5 kDa) was obtained from Nektar (Huntsville, AL). All other chemicals were of reagent grade and used as received. Purified water (obtained by passing house-distilled water through a Barnstead, E-pure water-purification system) was used to prepare all solutions.

Pore Etching and Nanotube Preparation. The same cell was used for etching, electrochemical determination of the dimensions of the pore, and for the resistive-pulse experiments.[43] It is a two-compartment Kel-F cell in which the PET membrane separates the two half cells. The damage track in the PET membrane was chemically etched into a conically shaped pore using the two-step etching method described in detail previously.[43] Conically shaped nanopores and tubes have two openings: the large-diameter (or base) opening at one face of the membrane and the small-diameter (or tip) opening at the opposite face (Figure 1A). We have shown that the two-step etching method provides for excellent reproducibility in both the tip and the base diameters.[43] The base diameter of the pores used for these studies was 520 nm, as determined by electron microscopy.[43]

The diameter of the tip opening was determined using an electrochemical method[42] described in detail in our prior work.[6,7] Briefly, the membrane containing the single conical nanopore was mounted in the cell, and an electrolyte solution of measured conductivity was placed on either side of the membrane. For these studies, this solution was 1 M KCl, pH 6 with a measured conductivity of 10 S/m. A current−voltage curve was obtained (Figure 2), the slope of which is the ionic conductance of the electrolyte-filled nanopore. The conductance is used to calculate the diameter of the tip opening.[6,7,42] The nanopores used

(40) Yu, S.; Lee, S. B.; Martin, C. R. *Anal. Chem.* **2003**, *75*, 1239−1244.
(41) Yu, S.; Lee, S. B.; Kang, M.; Martin, C. R. *Nano Lett.* **2001**, *1*, 495−498.
(42) Apel, P. Y.; Korchev, Y. E.; Siwy, Z.; Spohr, R.; Yoshida, M. *Nucl. Instrum. Methods Phys. Res., Sect. B* **2001**, *184*, 337−346.
(43) Wharton, J. E.; Jin, P.; Sexton, L. T.; Horne, L. P.; Sherrill, S. A.; Mino, W. L.; Martin, C. R. *Small* **2007**, *3*, 1424−1430.

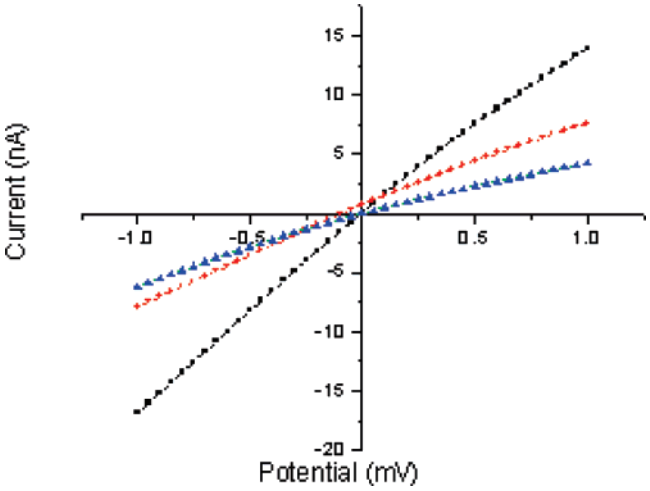

Figure 2. Current−voltage curves in 1 M KCl used to calculate the diameter of the tip opening after each step of the sensor-fabrication process. ■: As-prepared conical nanopore in the PET membrane. Red ●: After deposition of the conical gold nanotube. Blue ▲: After attachment of PEG to the nanotube walls.

for these studies had tip diameters, before deposition of the gold nanotube (vide infra) of 50 nm.

An electroless plating method[44] was then used to deposit gold along the pore walls to yield a correspondingly conically shaped gold nanotube within the pore (Figure 1). Electroless plating also yields gold surface films covering both faces of the membrane, but these were removed by swabbing the membrane faces with an ethanol-wetted cotton swab. A current−voltage curve obtained after plating was used to provide the diameter of the tip opening of the resulting gold nanotube (Figure 2). The diameter of the much larger base opening remained essentially unchanged after plating. Figure 1B shows an electron micrograph of such a conical gold nanotube. While in the sensing application the nanotube is left embedded in the PET membrane, to obtain this image the membrane was removed and the nanotube collected by filtration.[45]

PEG-thiol was attached to the gold surfaces to prevent nonspecific protein adsorption.[40,41] This was accomplished by immersing the nanotube membrane into a 0.1 mM solution of the PEG-thiol in purified water at 4 °C for ∼15 h. The membrane was then rinsed in purified water, and the diameter of the tip opening was remeasured (Figure 2). The tip diameters reported here are the diameters measured after PEG functionalization. Nanotubes with tip diameters between 9 and 27 nm were used for these studies. The current−voltage curve for the gold nanotube, before PEG functionalization, shows a nonzero current value at zero applied volts. Because the current is zero at an applied potential of 0 V before gold plating and after functionalization with PEG (Figure 2), the nonzero current value for the nanotube is most likely a result of residual capacitive current due to the higher capacitance of the unfunctionalized gold.

Current-Pulse Measurements. The membrane sample containing the PEG-functionalized conical gold nanotube was mounted in the cell, and both half cells were filled with ∼3.5 mL of 10 mM phosphate buffer solution (pH = 7.4) that was also 100 mM in KCl. A Ag/AgCl electrode (BAS, West Lafayette, IN) was placed into each half-cell solution and connected to an Axopatch 200B (Molecular Devices Corp., Union City, CA) patch-clamp amplifier. The Axopatch was used to apply the desired transmembrane potential and measure the resulting ion current flowing through the electrolyte-filled nanotube. The current was recorded in the voltage-clamp mode with a low-pass Bessel filter at 2 kHz bandwidth. The signal was digitized using a Digidata 1233A analogue-to-digital converter (Molecular Devices Corp.), at a sampling

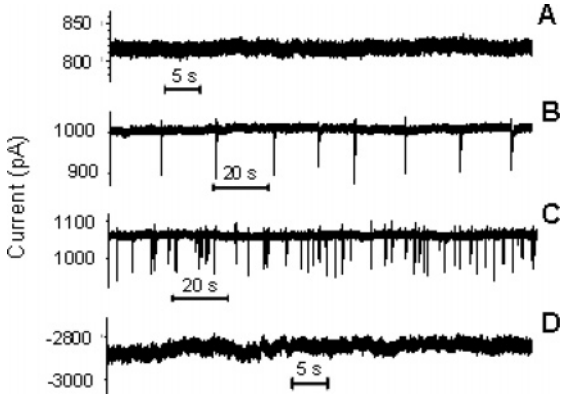

Figure 3. Current−time transients for a PEG-functionalized conical nanotube sensor with tip diameter = 17 nm. (A) Buffer only. (B) Buffer plus 50 nM BSA. (C) Buffer plus 100 nM BSA. Applied transmembrane potential for A, B, and C was 1000 mV. (D) Buffer plus 100 nM BSA at an applied transmembrane potential of −1000 mV.

frequency of 10 kHz. Data were recorded and analyzed using pClamp 9.0 software (Molecular Devices Corp.).

Unless otherwise stated, the applied transmembrane potential was 1000 mV with polarity such that the Ag/AgCl anode was in the half-cell solution facing the base opening, and the Ag/AgCl cathode in the solution facing the tip opening. Because the pI value of BSA is ∼4.8[46] and the pI of the control protein, SA, is ∼7.0,[47] both proteins have net negative charge in the pH = 7.4 buffer used here. While the exact pI of the anti-BSA-Fab is unknown, isoelectric focusing of whole polyclonal anti-BSA has shown pI values between 5.5 and 7.2.[48] All proteins were added to the half-cell solution facing the tip opening.

Finite Element Simulations. COMSOL Multiphysics v. 3.3a software (COMSOL, Inc.) was used to compute the electric field strength in and near the tip of the electrolyte-filled nanotube sensor. The software was run on a Dell OptiPlex GX520 (Pentium D CPU, 3.2 GHz, 2 GB RAM). Simulations of this type have been previously described.[49] COMSOL Multiphysics uses the finite element method to solve the partial differential equations that govern a system. Laplace's equation, $\nabla^2\phi = 0$, was solved for the electrostatic potential, ϕ.

The simulation included an electrolyte layer of 600 μm thickness on either side of the membrane with the electrolyte-filled conical nanotube between. The tube was assumed to be 12 μm long (the membrane thickness), with a base diameter of 520 nm. The tip diameter was varied from 10 to 25 nm. The tube was divided in two along its long axis (axis of symmetry), and the simulation was done for only one of the halves. Simulating half of the tube allowed us to use a larger number of elements, which improved accuracy. The number of elements used to compute each result was between 150 000 and 165 000.

Results and Discussion

Steady-State Current and Current-Pulse Data for BSA. In the absence of protein, a steady-state ion current (no current-pulse events) of ∼820 pA was observed for the PEG-functionalized nanotube with tip diameter of 17 nm (Figure 3A). As will be shown by the simulations (vide infra), conically shaped nanopores and tubes have an analyte-detection zone just inside the tip opening.[6,7,49] When BSA is added to the solution facing the tip opening, current pulses associated with electrophoretic transport of BSA through the detection zone were observed

(44) Menon, V. P.; Martin, C. R. *Anal. Chem.* **1995**, *67*, 1920−1928.
(45) Scopece, P.; Baker, L. A.; Ugo, P.; Martin, C. R. *Nanotechnology* **2006**, *17*, 3951−3956.
(46) Peng, Z. G.; Hidajat, K.; Uddin, M. S. *J. Colloid Interface Sci.* **2005**, *281*, 11−17.
(47) Haeuptle, M.-T.; Aubert, M. L.; Djiane, J.; Kraehenbuhl, J.-P. *J. Biol. Chem.* **1983**, *258*, 305−314.
(48) Maidment, B. W., Jr.; Papsidero, L. D.; Chu, T. M. *J. Immunol. Methods* **1980**, *35*, 297−306.
(49) Lee, S.; Zhang, Y.; White, H. S.; Harrell, C. C.; Martin, C. R. *Anal. Chem.* **2004**, *76*, 6108−6115.

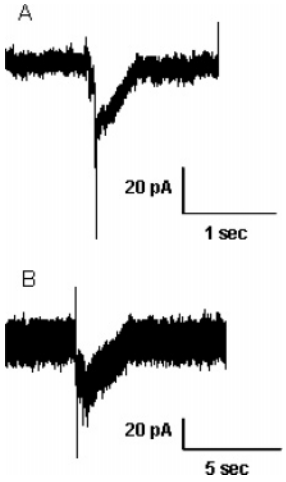

Figure 4. Expanded views of typical current pulses associated with tip-to-base translocation of (A) BSA (100 nM) and (B) BSA/anti-BSA-Fab ([BSA] = 100 nM, [anti-BSA-Fab] = 270 nM). Tip diameter = 17 nm. Transmembrane potential = 1000 mV.

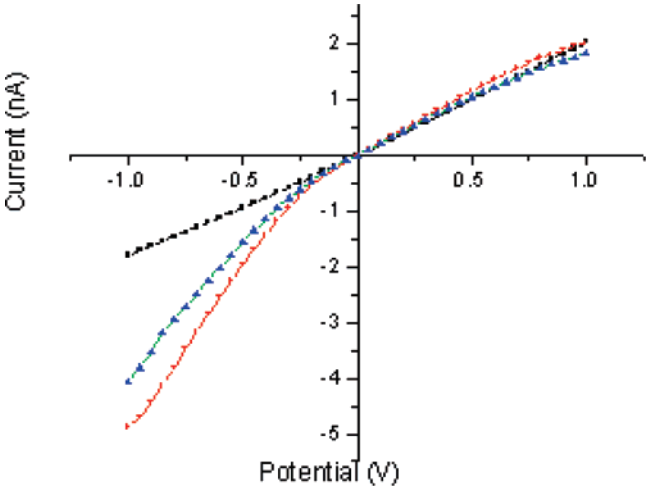

Figure 5. Effect of exposure to BSA on the current−voltage curves for a PEG-functionalized nanotube with tip diameter = 27 nm. ■: Before exposure, buffer only. Red ●: Buffer plus 100 nm BSA. Blue ▲: After removing the BSA solution, rinsing extensively, and returning to buffer only.

(Figure 3B). While we have not yet studied the concentration dependence in detail, as would be expected,[6,7,23,26,29,33] the current-pulse frequency is higher for higher BSA concentrations (Figure 3C). That these current pulses are due to electrophoretic transport is supported by the fact that when the polarity is reversed, no current pulses are observed (Figure 3D). This is because with this polarity, BSA is driven electrophoretically away from the nanotube membrane. As will be discussed below, the steady-state current is higher at reversed polarity (Figure 3D vs Figure 3A) because after exposure to BSA the nanotube acts as an ion current rectifier.[50−52]

Figure 4A shows an expanded view of a BSA current pulse. The current drops precipitously at the start and then tails upward with time. The duration of the pulse (τ) is defined as the time interval between the precipitous drop and the time when the current returns to the baseline value. The current-pulse amplitude (Δi) is the difference in current between the baseline value and the lowest current within the pulse. We have observed analogous current-pulse shapes for other charged analytes sent from tip-to-base through conically shaped nanotubes and pores, for example, for the BSA/anti-BSA complex (Figure 4B).[53] This shape is to be expected because the analyte is most effective at blocking the current when it is in the tip and least effective at blocking the current when it is far removed from the tip. Hence, the shape of the current pulse in principle could provide information about the length and geometry of the detection zone.

Close inspection of the current−time transients in Figure 3 reveals an unexpected result: The steady-state current (between pulses) in the presence of 100 nM BSA (1060 pA) is higher than the steady current in the presence of 50 nM BSA (1000 pA), which is higher than the steady current in the absence of BSA (820 pA). When the BSA solution was removed and replaced with buffer, the baseline current decreased to 860 pA but never returned to the lower pre-BSA-exposure value. To eliminate the possibility that the higher current observed in presence of BSA is due to a change in the conductivity of the buffer, we measured the buffer conductivity with and without 100 nM BSA. The conductivity was the same for both solutions.

To explore the origins of this interesting effect, we obtained current−voltage curves for the PEG-functionalized nanotube before and after exposure to 100 nM BSA (Figure 5). Before exposure, the current−voltage curve is linear, indicating that the PEG-functionalized nanotube is acting as an ohmic resistor, where the relevant resistance is that of the electrolyte-filled nanotube.[54] In the presence of 100 nM BSA, the current at both positive and negative potentials increases, but the increase at negative potentials is much more dramatic (Figure 5).

We obtained essentially identical results for unfunctionalized conical gold nanotubes before and after exposure to Cl^-.[50] Because Cl^- adsorbs to gold, after exposure the nanotube had fixed negative surface charge, and this charge was balanced by incorporating an equivalent number of cations from the electrolyte into the tube. These additional mobile cations made the ionic conductivity of the nanotube higher, and this accounted for the dramatic increase in current at negative potentials upon exposure to Cl^-.[50] As per Figure 5, a much smaller increase in current was observed at positive potentials. This is because nanotubes with small tip openings and fixed surface charge are ion-current rectifiers, which causes the current at positive potentials to be suppressed.[50]

That essentially identical results are observed upon exposure of the PEG-functionalized nanotubes to BSA indicates that, like Cl^-, the anionic BSA becomes attached to the nanotube walls. The most likely mechanism of attachment is via nonspecific adsorption to the underlying gold. While we attach PEG to the nanotube walls to suppress nonspecific adsorption,[40,41] the PEG monolayer consists, at best, of a close-packed array of the large PEG molecules across the gold surface. Because there is only one thiol per PEG molecule, this means that there is bare gold underneath the umbrella of the PEG molecules. Furthermore, it is unlikely that a perfectly close-packed PEG monolayer can be obtained, so BSA can access this bare gold through defects in the PEG layer.

(50) Siwy, Z.; Heins, E.; Harrell, C. C.; Kohli, P.; Martin, C. R. *J. Am. Chem. Soc.* **2004**, *126*, 10850−10851.
(51) Harrell, C. C.; Kohli, P.; Siwy, Z.; Martin, C. R. *J. Am. Chem. Soc.* **2004**, *126*, 15646−15647.
(52) Heins, E. A.; Baker, L. A.; Siwy, Z. S.; Mota, M. O.; Martin, C. R. *J. Phys. Chem. B* **2005**, *109*, 18400−18407.
(53) Unpublished work from the Martin group, 2007.
(54) Harrell, C. C.; Lee, S. B.; Martin, C. R. *Anal. Chem.* **2003**, *75*, 6861−6867.

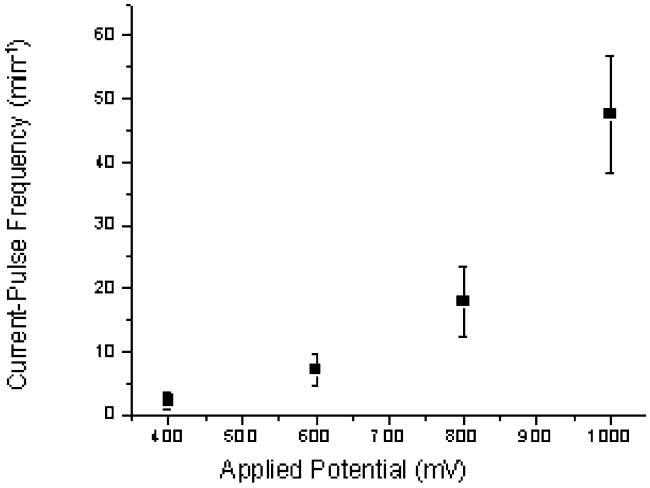

Figure 6. BSA current-pulse frequency versus transmembrane potential. Tip diameter = 17 nm. [BSA] = 500 nM. Error bars represent standard deviations obtained by averaging the number of pulses in four 5-min windows of the current-pulse data.

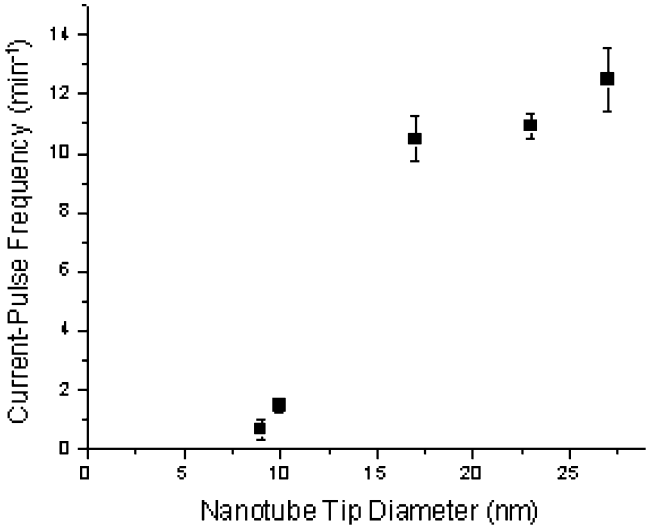

Figure 7. BSA current-pulse frequency versus nanotube tip diameter. [BSA] = 100 nM. Applied transmembrane potential = 1000 mV.

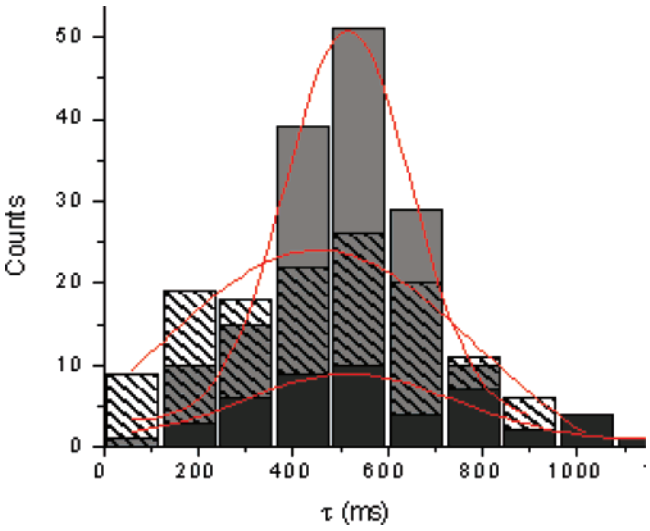

Figure 8. Histograms of BSA current-pulse-duration data for nanotubes with three different tip diameters. Tip diameters were: dark gray, 9 nm; light gray, 17 nm; hatched, 27 nm. Solid curves are Gaussian fits. [BSA] = 100 nM. Applied transmembrane potential = 1000 mV.

This nonspecific adsorption argument is supported by the fact that the initial linear I−V curve cannot be regenerated by rinsing and soaking in pure buffer (Figure 5). If BSA simply partitioned into the PEG, we would expect this process to be completely reversible. It is interesting to note, however, that in our prior work on PEG-functionalized gold nanotubes,[41] we conducted protein transport experiments over a 5-day period without any evidence for nonspecific adsorption. That a small amount of nonspecific adsorption can be detected by the current−voltage-curve measurement (Figure 5) shows how sensitive this electrochemical method is to adsorbed surface charge.

Effect of Potential on Current-Pulse Frequency. The pulse frequency (f_p) was determined by counting the number of pulses in 5-min windows (e.g., Figure 3B) and then averaging the counts from four such windows. In analogy to data obtained for other charged analytes with both artificial[6,7] and biological[32] nanopores, there is a threshold voltage below which BSA current pulses are not observed, and f_p increases exponentially with applied potential above this threshold (Figure 6). This is because the BSA molecule pays an entropic penalty when it enters a pore with a tip opening of comparable size to the molecule.[6,7,32] Because BSA is charged, this entropic barrier can be overcome by driving the BSA molecule electrophoretically into the nanotube tip.[6,7,32]

Effect of Tip Diameter on BSA Current-Pulse Frequency and Duration. The BSA molecule is shaped roughly like an American football with a long axis of ~14 nm and a short axis of ~4 nm.[46] When the tip diameter is smaller than the 14-nm long axis, f_p is low, but there is a jump in f_p for tips with diameters larger than the long axis (Figure 7). This again reflects the entropic penalty paid by the molecule when it enters the tip. The penalty is higher for tips with diameters smaller than the 14-nm BSA long axis because the BSA molecule loses a degree of rotational freedom in such very small tips.

Figure 8 shows a histogram of BSA current-pulse duration (τ) data obtained for nanotubes with three different tip diameters. Each histogram was fitted to a Gaussian distribution (solid curve),[14,27,34,35,37] which provided the average pulse duration and standard deviation of the average. Tips with diameters of 9, 17, and 27 nm gave pulses with average τ values of 520 ± 190, 520 ± 110, and 450 ± 290 ms, respectively. A similar independence of τ on pore diameter was observed for DNA translocation through a synthetic nanopore sensor.[11]

A qualitative explanation for this interesting result can be obtained by considering the electrophoretic velocity, v, of a charged analyte molecule, which is given by[55]

$$v = |z|eE/6\pi\eta r \qquad (1)$$

where z and r are the charge and radius of the analyte, respectively, e is the electronic charge, E is the electric field strength, and η is the solution viscosity. The term in the denominator is the molecular friction that opposes transport,[56,57] which is related to the diffusion coefficient (D) by the Stokes−Einstein equation

(55) Bard, A. J.; Faulkner, L. R. *Electrochemical Methods*, 2nd ed.; John Wiley & Sons: New York, 2001; p 66.
(56) Martin, C. R.; Nishizawa, M.; Jirage, K.; Kang, M. *J. Phys. Chem. B* **2001**, *105*, 1925−1934.
(57) Deen, W. M. *AlChE J.* **1987**, 1409−1425.

$$D = kT/6\pi\eta r \quad (2)$$

Substituting eq 2 into eq 1 gives

$$\upsilon = |z|eED/kT \quad (3)$$

Taking the reciprocal of both sides and multiplying by the length of the detection zone, l_t, for our nanotube sensor, provides the following equation for the current pulse duration, τ:

$$\tau = l_t kT/|z|eED \quad (4)$$

Equation 4 shows that if τ is independent of tip diameter (Figure 8), then the product E*D* must be independent of tip diameter.

To test this prediction, we need values for the diffusion coefficient for the BSA molecule in the nanotube tip, D_{tip}. D_{tip} is less than the diffusion coefficient in bulk solution because the molecular friction term is larger in the tip due to collisions of the BSA with the nanotube walls (i.e., hindered diffusion).[56,57] D_{tip} can be calculated using the Renkin equation[56,57]

$$\frac{D_{tip}}{D_{sol}} = 1 - 2.104\lambda + 2.09\lambda^3 - 0.95\lambda^5 \quad (5)$$

where D_{sol} is the diffusion coefficient in bulk solution,[58] and λ is the ratio of the diameter of the BSA molecule to the diameter of the nanotube tip. We used the 4 nm short-axis diameter of BSA in these calculations. Table 1 shows D_{tip} values for nanotubes with tip diameters in the range of 10−25 nm. As expected, D_{tip} decreases with decreasing tip diameter.

The electric field strength in the nanotube tip can be calculated via finite-element simulation.[49] Figure 9A shows the results for a nanotube with tip diameter of 17 nm and base diameter of 520 nm. While the applied transmembrane potential was only 1 V, the field strength just inside the tip is nearly 2 MV m^{-1}. Furthermore, Figure 9B shows that field strength in the tip increases linearly with the reciprocal of the tip diameter. The product of ED_{tip} is shown in the last column of Table 1, and we see, as predicted, that this product is nearly independent of tip diameter.

There are, however, two caveats. First, the calculation uses the values of *E* and D_{tip} just inside the tip. Yet because the nanotube diameter becomes larger from tip to base, the diffusion coefficient (*D*) will increase, and *E* will decrease, as the BSA molecule translocates. Interestingly, again we see the offsetting effects of *D* and *E*. Second, because *E* is linearly related to the reciprocal of the tip diameter (Figure 9B), and the relationship between D_{tip} and diameter is nonlinear (eq 5), ED_{tip} will be constant only over a limited range of tip diameters.

Current-Pulse Data for SA, SA/anti-BSA-Fab, and BSA/anti-BSA-Fab. A histogram of τ data for a solution that was 100 nM in the control protein SA (Figure 10A) provided an average current-pulse duration of τ_{SA} = 470 ± 140 ms. The histogram for a solution that was 100 nM in the anti-BSA-Fab (Figure 10B) provided an average current-pulse duration of τ_{Fab} = 400 ± 110 ms.

Because SA is not bound by the anti-BSA-Fab, a solution that contains both of these proteins should show current pulses for the free SA and for the free Fab. However, because the average pulse durations for these two proteins are the same

Table 1. Calculated Diffusion Coefficient for BSA in the Nanotube Tip, and Simulated Electric Field Strength in the Tip, for Nanotubes with the Indicated Tip Diameters (See Text and Eq 5 for Details)

tip diameter (nm)	λ	D_{tip} ($\times 10^{-7}$ cm^2 s^{-1})[a]	E (MV m^{-1})[b]	$D_{tip}E$ ($\times 10^{-3}$ cm V s^{-1})
10	0.40	1.7	3.2	5.4
15	0.27	2.8	2.2	6.2
20	0.20	3.6	1.6	5.8
25	0.16	4.1	1.3	5.3

[a] Calculated using eq 5, with a value of 6×10^{-7} cm^2 s^{-1} for D_{sol}.[58] [b] Value obtained from finite-element simulations using a base diameter of 520 nm.

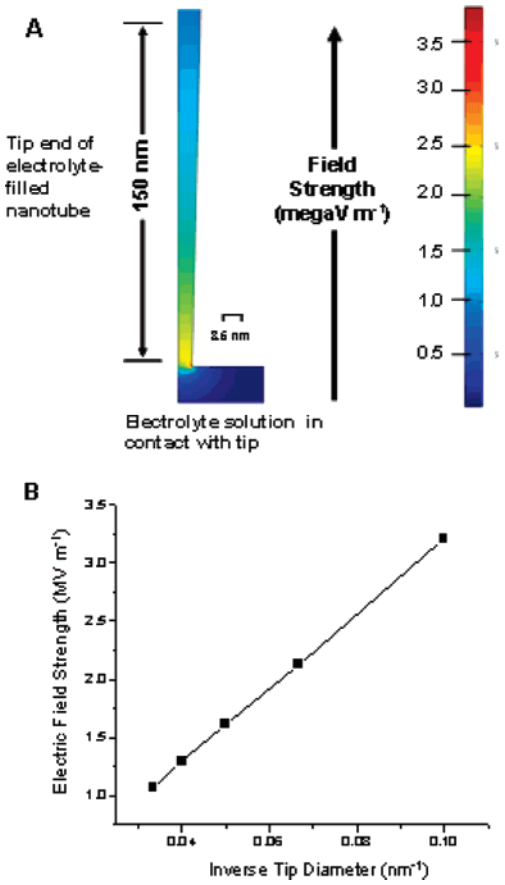

Figure 9. (A) Finite-element simulation of electric field strength in and near the tip opening for a nanotube with base opening = 520 nm and tip opening = 17 nm. Membrane thickness = 12 μm. Applied transmembrane potential = 1000 mV. (B) Plot of electric field strength in the nanotube tip obtained from such simulations versus the inverse of the tip diameter.

(Table 2), the current-pulse data for the SA/anti-BSA-Fab solution show only one population of current pulses (Figure 11A). An average pulse duration of 460 ± 120 ms was obtained, identical to τ_{Fab} and τ_{SA} (Table 2).

The situation for a solution containing both BSA and the anti-BSA-Fab should be different because the Fab binds BSA to yield a complex (vide infra) that is larger than any of the individual proteins. Studies of DNA translocation through biological[33,37] and artificial[11,17] nanopore sensors have shown that both the average current-pulse duration and the standard deviation of the average increase with the size of the DNA.[11,17,33,37] These results suggest that we should see longer duration current pulses, and larger standard deviations, for solutions containing both BSA and the anti-BSA-Fab. The histogram for a solution that was 100 nM in BSA and 270 nM

(58) Gaigalas, A. K.; Hubbard, J. B.; McCurley, M.; Woo, S. *J. Phys. Chem.* **1992**, *96*, 2355−2359.

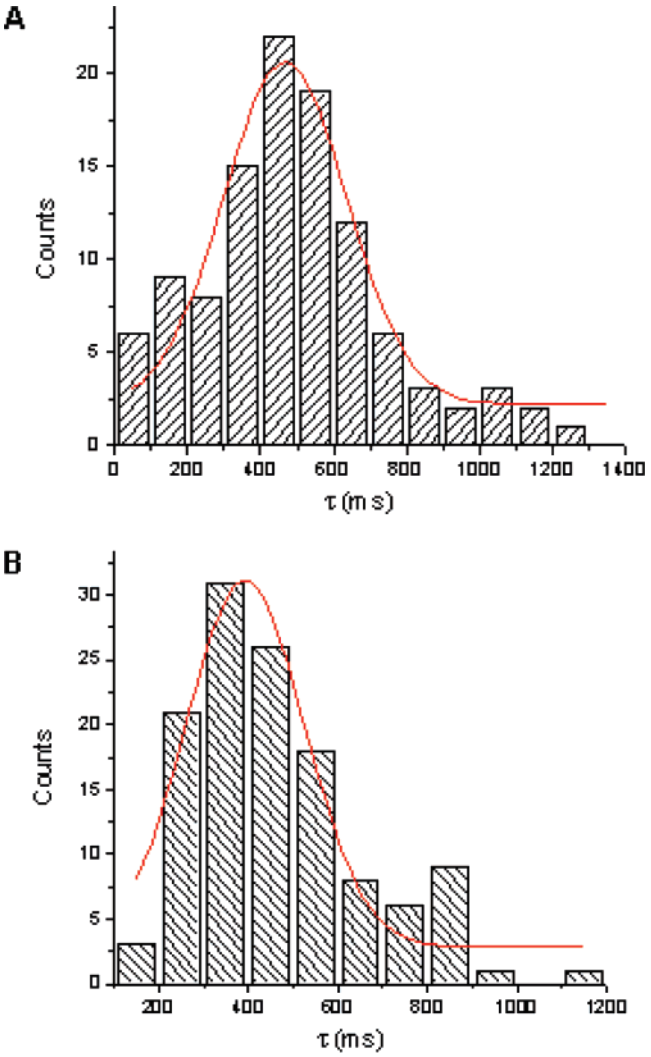

Figure 10. Histograms of current-pulse-duration data. (A) 100 nM SA. (B) 100 nM anti-BSA-Fab. Solid curves are Gaussian fits. Applied transmembrane potential = 1000 mV. Tip diameter = 17 nm.

Table 2. Current-Pulse-Duration (τ) Data for the Indicated Proteins and Protein Mixtures[a]

protein(s)	concentration (nM)	τ (ms)
BSA	100	520 ± 110
SA	100	470 ± 140
anti-BSA-Fab	100	400 ± 110
SA/anti-BSA-Fab	100/200	460 ± 120
BSA/anti-BSA-Fab	100/270	2200 ± 650
BSA/anti-BSA-Fab (27 nm tip)	100/90	1070 ± 220

[a] Unless otherwise noted, the tip diameter was 17 nm.

in the anti-BSA-Fab (Figure 11B) shows that this is the case, yielding an average pulse duration for this BSA/anti-BSA-Fab mixture of 2200 ± 650 ms (Table 2).

That addition of anti-BSA-Fab yields a complex that is larger than the free BSA is further verified by the current-pulse frequency data. Prior to addition of the Fab, a nanotube with a 17 nm tip gave f_p for the 100 nM BSA solution of 10.5 ± 0.8 min^{-1} (Figure 3C), but after addition of 270 nM Fab f_p was 1.2 ± 0.4 min^{-1} (Figure 12). This drop in frequency occurs because the activation energy for entry of the larger complex into the nanotube tip is higher than the activation energy for the free BSA.

There is, however, an interesting point that requires further discussion. The current-pulse data summarized in Figure 11B were obtained for a solution that was 100 nM in BSA and 270 nM in the anti-BSA-Fab. If the stoichiometry of binding between the BSA and the anti-BSA-Fab were 1:1, the solution should be ~100 nM in the complex BSA_1/anti-BSA-Fab_1 and ~170 nM in excess anti-BSA-Fab. This would suggest that we should see two populations of current pulses, one with an average duration of 400 ms for the excess anti-BSA-Fab and one with longer pulse duration for the complex. Furthermore, again assuming 1:1 stoichiometry, there should be ~1.7 times as many of the short-duration pulses. This is not observed experimentally. Indeed, there is no clear evidence for a set of short duration (~400 ms) current pulses in Figure 11B.

To understand why this is, it is important to point out that BSA is a multivalent antigen; that is, a single BSA molecule can bind more than one anti-BSA.[59−66] The size and composition of the BSA/anti-BSA complexes formed depend on the relative concentrations of BSA and anti-BSA in solution. A variety of methods have been used to study complex size in the presence of excess antibody. For example, quasi-elastic light scattering was used to determine complex size in the presence of three different monoclonal antibodies, which bound to different epitopes on the BSA molecule.[60,61] When all three antibodies were present, the average size of the BSA/anti-BSA complex was larger than when only two were present, showing that BSA can bind up to three anti-BSA molecules.[60]

Similar studies were conducted using sucrose density gradient ultracentrifugation to determine complex size.[62] These studies showed that the maximum complex size occurred in solutions containing a large excess of antibody.[62] Studies have also been conducted with polyclonal antibodies and BSA using size-exclusion high performance liquid chromatography.[63] Complex size was investigated in solutions containing up to 9 times antibody excess and 9 times antigen excess. The largest BSA/anti-BSA complexes formed when a 3-fold excess of antibody was used.[63] Other studies done with whole polyclonal antibodies showed that when BSA was in low to moderate degrees of excess, the predominant complex formed was BSA_1/anti-BSA_1.[64] These studies also found that a small amount of BSA_2anti-BSA_1 formed with excess BSA. This is to be expected because the whole antibody is bivalent. This would not be possible with the anti-BSA-Fab used here.

The results of these previous investigations suggest that the predominant complex in the solution containing 100 nM BSA and 270 nM anti-BSA-Fab (Figure 11B) has stoichiometry BSA_1/anti-BSA-Fab_3. This explains why we do not see current pulses due to the free Fab in Figure 11B. These prior studies would also suggest that if solutions with ~1:1 stoichiometry were used, the smaller BSA_1/anti-BSA-Fab_1 complex would

(59) Benjamin, D. C.; Teale, J. M. *J. Biol. Chem.* **1978**, *253*, 8087−8092.
(60) Yarmush, D. M.; Murphy, R. M.; Colton, C. K.; Fisch, M.; Yarmush, M. L. *Mol. Immunol.* **1988**, *25*, 17−32.
(61) Murphy, R. M.; Slayter, H.; Schurtenberger, P.; Chamberlin, R. A.; Colton, C. K.; Yarmush, M. L. *Biophys. J.* **1988**, *54*, 45−56.
(62) Hosoi, S.; Shinomiya, K.; Mikawa, H. *Clin. Immunol. Immunopathol.* **1984**, *32*, 378−386.
(63) Holmskov-Nielsen, U.; Jensenius, J. C.; Erb, K.; Husby, S. *Immunology* **1984**, *51*, 809−814.
(64) Arend, W. P.; Teller, D. C.; Mannik, M. *Biochemistry* **1972**, *11*, 4063−4072.
(65) Chiem, N. H.; Harrison, D. J. *Electrophoresis* **1998**, *19*, 3040−3044.
(66) Steensgaard, J.; Jacobsen, C.; Lowe, J.; Ling, N. R.; Jefferies, R. *Immunology* **1982**, *46*, 751−760.

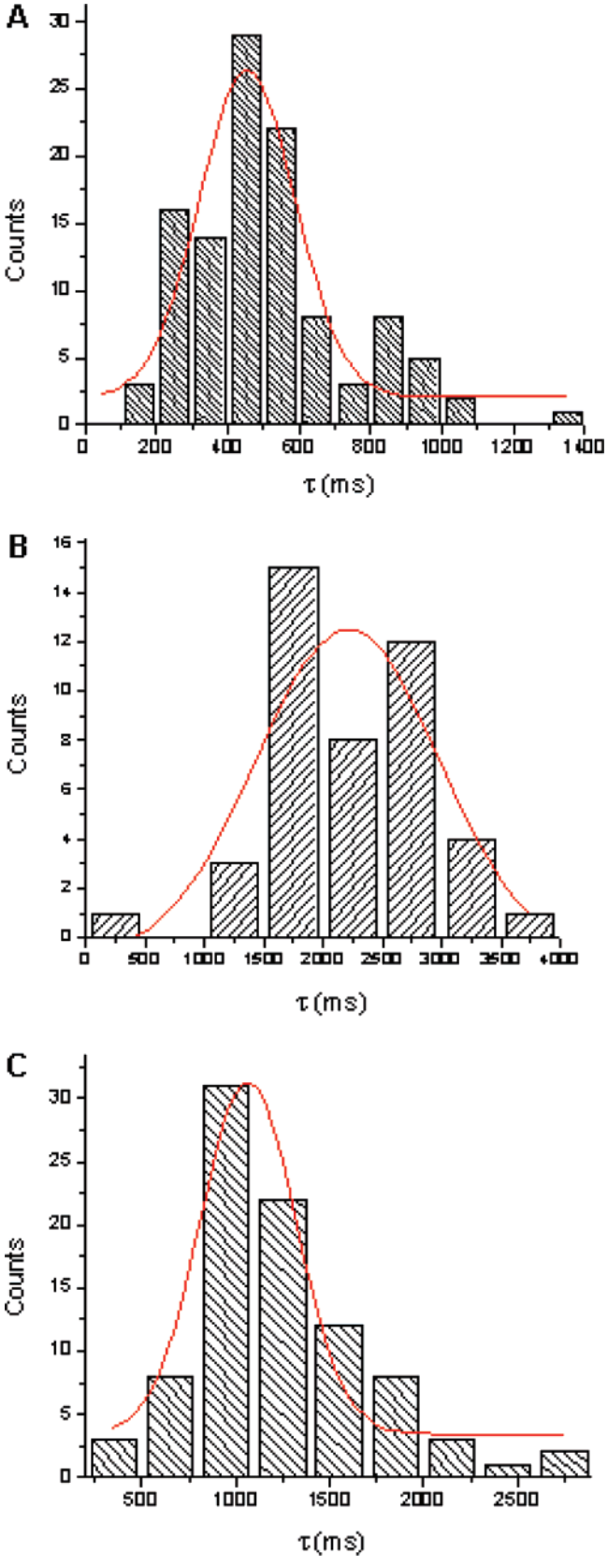

Figure 11. Histograms of current-pulse-duration data. (A) 100 nM SA plus 200 nM anti-BSA-Fab. (B) 100 nM BSA plus 270 nM anti-BSA-Fab. (C) 100 nM BSA plus 90 nM anti-BSA-Fab. Solid curves are Gaussian fits. Applied transmembrane potential = 1000 mV. Tip diameter for (A) and (B) is 17 nm. Tip diameter for (C) is 27 nm.

Figure 12. Current−time transient for a PEG-functionalized conical nanotube sensor with a solution 100 nM in BSA and 270 nM in anti-BSA-Fab on the tip side of the membrane. Tip diameter = 17 nm. Transmembrane potential = 1000 mV.

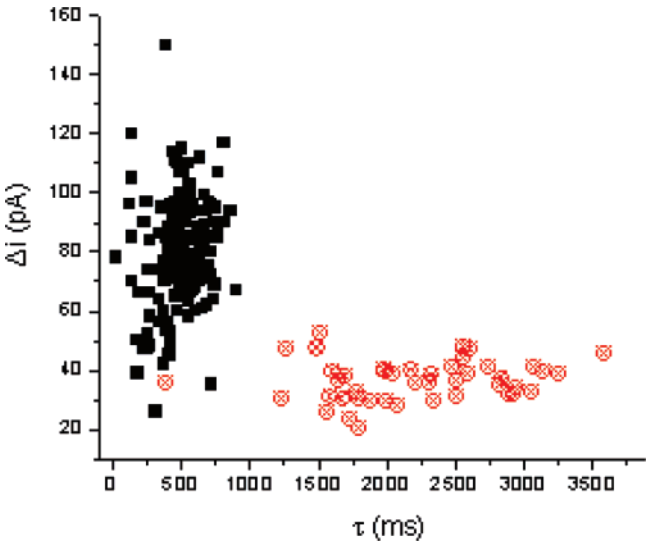

Figure 13. Scatter plot of current-pulse magnitude (Δi) versus current-pulse duration (τ) for 100 nM BSA only (black) and 100 nM BSA plus 270 nM anti-BSA-Fab (red). Applied transmembrane potential = 1000 mV. Tip diameter = 17 nm.

predominate, and a shorter average current-pulse duration would be observed. Figure 11C shows that this is indeed the case (Table 2).

Scatter Plot. Scatter plots of current pulse amplitude, Δi, versus current-pulse duration, τ, are often used to summarize resistive-pulse data.[6,11,12,17,24,35,38] The scatter plot for a solution that was 100 nM in BSA before and after adding 270 nM anti-BSA-Fab (Figure 13) shows that it is easy to distinguish the pulses for the BSA/anti-BSA-Fab complex from the pulses for the free BSA. These data also reinforce the point that the spread in τ values for the complex is larger than that for the free BSA. These results prove the major premise of this work, that a unique current-pulse signature can be obtained when an antibody that binds an analyte protein is added to a solution containing this protein. Furthermore, the control studies with SA/anti-BSA-Fab solutions show that a protein that does not bind to the antibody does not yield this unique set of current pulses.

However, a perplexing issue arises from the scatter plot: Why does the larger BSA/anti-BSA-Fab complex show current pulses of smaller Δi than the pulses for the free BSA? This is perplexing because one might expect the larger BSA/anti-BSA-Fab complex to be more effective at blocking the nanotube tip than the smaller free BSA. As a result, a larger Δi would be anticipated for the complex. This argument assumes, however, that resistive-pulse sensing of a molecule in a nanopore is completely analogous to resistive-pulse sensing of a particle with the well-known Coulter counter.[2] In the Coulter case, it is simply assumed that the particle displaces a volume element of

electrolyte solution in the pore, and, as a result, the resistance of the pore always increases when the particle is present.

There have been two recent reports that indicate that this simple pore-blocking analogy is not always applicable to molecular resistive-pulse sensing.[20,21] In both of these studies, DNA analytes produced upward, as opposed to downward current pulses; that is, the resistance of the nanopore decreased when the DNA analyte was in the pore. These results were interpreted by noting that when a highly charged analyte enters the nanopore, it must bring its charge-balancing counterions with it. As result, there is a transient introduction of additional charge carriers when the analyte is in the nanopore, and this accounts for the upward current pulses.[20,21] It is possible that smaller amplitude current pulses are observed for the BSA/anti-BSA-Fab complex, relative to free BSA, because the increased size (makes amplitude larger) is partially compensated for by an increase in charge (makes amplitude smaller) as the complex translocates the nanopore tip. Another possibility is that the conformation of the protein changes upon binding by the Fab, which makes the complex less effective at blocking the tip. Further studies will be necessary before a definitive conclusion can be reached.

Conclusions

We have demonstrated that nanotube resistive-pulse sensors can be used to detect protein analytes and that selectivity can be obtained by adding an antibody to the target protein to the analyte solution. We have also shown that the current-pulse signature for the protein/antibody complex can be used to obtain information about the size of this complex. Hence, the resistive pulse-sensor can be used as a tool to study the stoichiometry of binding between an antibody and an antigen[19] or, in general, between a ligand and a receptor. We have also shown that, because the tip diameter of nanotube sensors prepared by the track-etch method can be controlled at will,[43] the size of the tip can be optimized for detection of the desired analyte (Figure 7). In addition, with this technology we have the ability to conveniently measure the size of the tip after each step of the fabrication process (Figure 2).

The key to obtaining current pulses for the free BSA and for the BSA/anti-BSA-Fab complex is using a nanotube with a tip diameter comparable to the diameter of these species (10−20 nm). Uram et al. have demonstrated a similar protein-sensing concept using much larger pores (575 nm) prepared by a laser-boring method.[19] Because a much larger pore was used, they could only detect very large protein/antibody complexes consisting of 610−17 300 proteins. Such large complexes formed because Uram et al. used the whole antibody as opposed to the Fab fragment used here.[19]

The use of gold as the nanotube material is advantageous because gold can be easily functionalized, for example, to suppress nonspecific protein adsorption, as was done here. Furthermore, the sensor can be evaluated after exposure to the analyte to see if irreversible changes in the device have occurred (Figure 5). In addition, the abilities to model the nanotube (Figure 9A) and to explore how tube geometry influences field strength in the nanotube tip (Figure 9B) are important features of this technology. We believe these results indicate that gold nanotube resistive-pulse sensors prepared by the track-etch method show promise for development into a practical protein sensing devices.

Acknowledgment. This work was supported by the Army Research Office (ARO) and the National Science Foundation (CHE-9987646).

JA0739943